International Journal of Thermophysics, Vol. 15, No. 6, 1994

A Small-Angle Neutron Scattering (SANS) Study of Worm-like Micelles Under Shear[1]

M. Y. Lin,[2] H. J. M. Hanley,[3,4] G. C. Straty,[3] D. G. Peiffer,[2] M. W. Kim,[2] and S. K. Sinha[2]

The structure of a cationic worm-like cylindrical micelle was investigated by SANS (small-angle neutron scattering). Intensities from 0.1% by weight solutions in D_2O, at rest and under shear, were measured on the NIST Cold Neutron Research Facility 30-m spectrometer in the wave vector range $0.03 \leqslant Q\ (\text{nm}^{-1}) \leqslant 2.0$. Scattered intensity patterns from the solutions subjected to shears equal to or greater than $40\ \text{s}^{-1}$ showed pronounced anisotropy, but such anisotropy could not be detected below this apparent threshold shear. The threshold was characterized by a relaxation time since anisotropy was detected only after several minutes of shearing. In contrast, the anisotropy was apparent immediately the shear was applied at the higher shears. The data were analyzed based on the assumption that the micelles behave as rigid rods. Estimates of the radii and length under shear are given. Polydispersity in rod length is discussed, and we argue that it contributes significantly to the scattering patterns.

KEY WORDS: anisotropy; Couette flow; living polymers; polydispersity; rods; shear alignment; small-angle neutron scattering; worm-like micelles.

1. INTRODUCTION

This paper reports preliminary findings from a SANS (small-angle neutron scattering) experiment on a micellar solution. Our sample is a variant of the class of micelles composed of a cationic surfactant and counter ion, usually a bromine or aromatic salt [1]. The micelles have interesting

[1] Paper presented at the Twelfth Symposium on Thermophysical Properties, June 19–24, 1994, Boulder, Colorado, U.S.A.

[2] Exxon Research and Engineering Company, Annandale, New Jersey, U.S.A.

[3] Thermophysics Division, National Institute of Standards and Technology, Boulder, Colorado 80303, U.S.A.

[4] To whom correspondence should be addressed.

0195-928X/94/1100-1169$07.00/0 © 1994 Plenum Publishing Corporation

structures and properties. Initially spherical at very low surfactant concentrations, they transform and undergo uniaxial growth to become worm-like cylindrical aggregates that can attain lengths of several hundred nanometers as the concentration is increased. With, in particular, a salicylate as the counter ion, their aqueous solutions are highly viscous and non-Newtonian at even moderate concentrations [2, 3]. Unlike a conventional polymer, however, the worms—sometimes called "living polymers"—break and reform continuously. The solution is thus stable when subjected to an extremely high mechanical stress, and its properties recover when the stress is removed.

The motivation of this work was twofold: first, to clarify the shape and growth pattern of the micelles using SANS data taken from the solution under shear [4, 5] and, second, as a preliminary to a long-range program which will probe the structure of inorganic/organic particulate systems by neutron, light, and x-ray radiation. Our sample is the organic component of a micelle/clay mix that is presently under study [6].

2. EXPERIMENTS

2.1. The Sample

The surfactant was prepared by an equimolar reaction of allyl bromide with dimethyl hexadecylamine in a polar solvent (dimethylformamide) at 323 K. The product is isolated by adding acetone and subsequently dried. The micellar solution was made up by mixing 0.1 g surfactant/dl (0.025 M) with an equimolar amount of sodium salicylate in D_2O. Surface tension measurements indicate a critical micelle concentration of $\sim 0.002\%$, and viscosity data suggest a C^* (overlap concentration) of $\sim 0.15\%$.

2.2. SANS Measurements

SANS data were taken at the NIST Cold Neutron Research Facility on the NG7 30-m spectrometer configured to a wavelength $\lambda = 0.5$ nm and sample-to-detector distances of 15 and 5 m. With the solution in a quartz cell of path length 1 mm, scattered intensities, $I(Q)$, were recorded as a function of the scattered wave vector Q [$Q = (4\pi/\lambda) \sin \theta/2$, where λ is the incident neutron wavelength, and θ the scattering angle] over the range $0.03 \leqslant Q/\text{nm}^{-1} \leqslant 1.5$, corrected for the cell contribution, background, and detector variation, and put on an absolute scale by comparing to a NIST standard. For the shear studies, the SANS instrument was configured with the NIST 1-mm-gap width Couette shearing cell [7] in the sample position. In Cartesian coordinates, the neutron beam is incident along the Y axis and the intensity is measured as a function of $\mathbf{Q}$ in the x–z plane.

Under shear, the flow velocity (**u**) is the x direction, and the shear rate is defined as $\dot{\gamma} = \partial u_x/\partial y$. Shearing data were corrected as before. The data were presented as two-dimensional images and angle averaged or sector averaged, depending on whether or not anisotropy was observed in the two-dimensional patterns.

3. RESULTS

The essential scattering information is represented by Figs. 1 to 3. Shown are the scattering patterns from the sample in the shearing cell at $\dot{\gamma} = 0$, 40, and 80 s^{-1}. The plot at zero shear is radially symmetric, but the radial symmetry is lost as the shear increases and the pattern becomes elliptical. The progression, however, from circle to ellipse was not continuous with increasing shear. A plot of the parameter $[I(90) - I(0))/I(0)]$ as a function of shear (where $I(90)$ and $I(0)$ are the intensities at 90 and 0° in the x–z scattering plane), and the appearance of the patterns themselves indicated no anisotropy if $\dot{\gamma} < 40\ s^{-1}$. Furthermore, at this threshold, the pattern became anisotropic only after shearing for 6–8 min. Above the threshold, the pattern became more and more elliptic with increasing shear until the pattern appeared to reach saturation at 80 s^{-1}. Anisotropy at these higher shears was seen immediately on applying the shear.

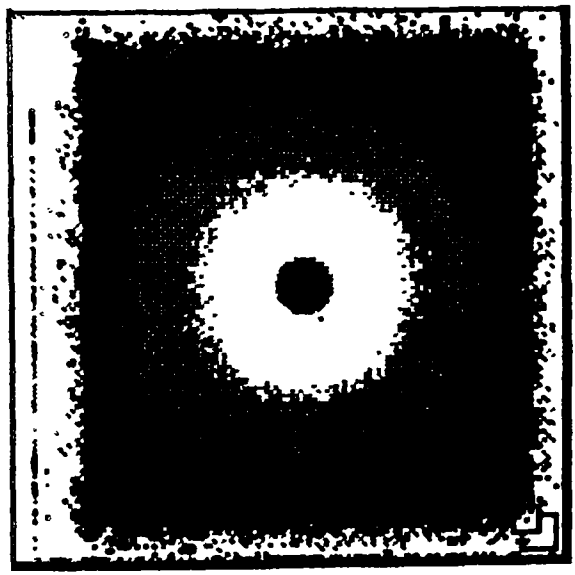

Fig. 1. Scattered intensity plot from the micellar solution at zero shear.

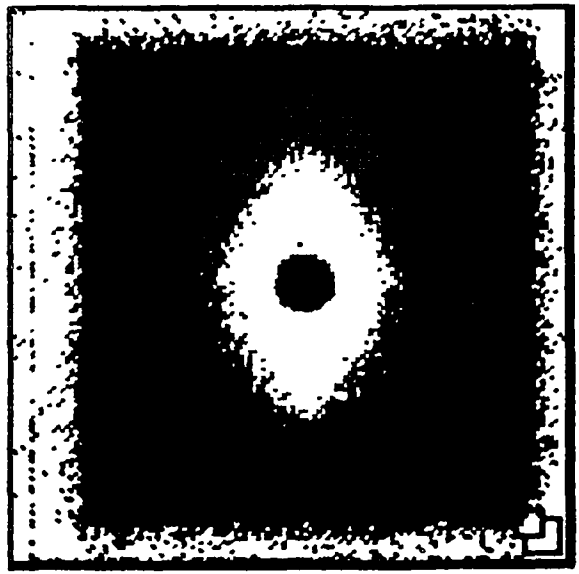

Fig. 2. Scattered intensity plot (see text) from the micellar solution under a shear, $\dot{\gamma} = 40\ s^{-1}$. Note the strong anisotropy but the thick waist at small Q.

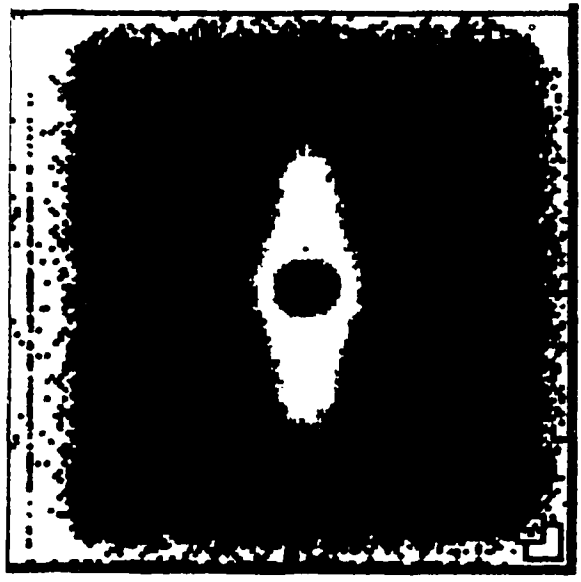

Fig. 3. Scattered intensity plot from the micellar solution under a shear, $\dot{\gamma} = 80\ s^{-1}$.

4. ANALYSIS

Since the concentration of our micelle solution is less than the C^* value, we assume that the system can be approximated by a system of non-interacting rods. The equations representing scattering from a rod under shear [4–6, 8, 9] are as follows.

Consider the standard coordinate system [4] in which the orientation of the rod is given by polar angles θ and ϕ; $\mathbf{Q}$ rotates through angle ψ in the plane of the detector (the x–z plane), and β is defined as the angle between the vector $\mathbf{Q}$ and the rod axis. The intensity is thus,

$$I(\mathbf{Q}) = \text{Const} \frac{\int_0^{2\pi} d\psi \int_0^{2\pi} d\phi \int_0^{\pi} p(\theta, \phi; \Gamma) F^2(Q, \beta) \sin\theta \, d\theta}{\int_0^{2\pi} d\psi \int_0^{2\pi} d\phi \int_0^{\pi} p(\theta, \phi; \Gamma) \sin\theta \, d\theta} \tag{1}$$

Here the prefactor represents the product of an apparatus constant, a term proportional to the concentration of surfactant molecules, the micelle aggregation number, and the scattering length density of the micelles with respect to that of the medium [8]. The function $F(Q, \beta)$ is the average form factor given by [9]

$$F(Q, \beta) = \left(\frac{\sin(QL\cos\beta)}{QL\cos\beta}\right) \frac{j_1(Qa\sin\beta)}{Qa\sin\beta} \tag{2}$$

for a rigid rod of length $2L$ and diameter $2a$; $j_1(x)$ is the first-order Bessel function of the first kind. The neutron beam traverses the sample twice in the experimental shear cell, so the direction of the shear gradient in the forward and back illuminated segment is reversed; hence

$$F^2(Q, \beta) = F^2(Q, \beta_+) + F^2(Q, \beta_-) \tag{3}$$

with

$$\cos\beta_\pm = \sin\theta\cos\phi\cos\psi \pm \cos\theta\sin\psi \tag{4}$$

Equation (1) includes the probability $p(\theta, \phi, \Gamma)$ that the rod will orient to a particular (θ, ϕ) for a given value of the parameter Γ, where $\Gamma = \dot{\gamma}/D_r$, with D_r the rotational diffusion coefficient. Here we assume the Hayter–Penfold expression [4] for the probability function and refer to their paper for a background discussion, see also Ref. 6:

$$p(\theta, \phi; \Gamma) = \left(\frac{1}{4\pi}\right) \frac{(1 - \cos 2\phi_0)(1 + \sin^2\theta\cos 2\phi_0)^{3/2}}{(1 - \sin^2\theta\cos 2\phi_0\cos 2(\phi - \phi_0))^2} \tag{5}$$

where $2\phi_0 = \tan^{-1}(8/\Gamma)$.

4.1. Zero-Shear Data

The circularly averaged intensity from the sample at rest is shown in Fig. 4 as the filled circles. That the system has essentially the same morphology until a threshold shear is exceeded is supported by the intensity at $30\,s^{-1}$ (open circles). Figure 4 also shows that the power-law slope of the intensity with Q is -1 over a wide range of Q, which suggests that the micelles are rod-like. This conclusion at first sight seemed unrealistic since the micelles are so long and are known to break and reform. Nevertheless, a simple calculation appears to rule out obvious alternative structures. Suppose, for example, the micelle coiled to become an effective sphere of radius R; the form factor is the standard expression [9], $(F(Q))^2 = [(3/x^3)(\sin x - x\cos x)]^2$, where $x = QR$. Or suppose the

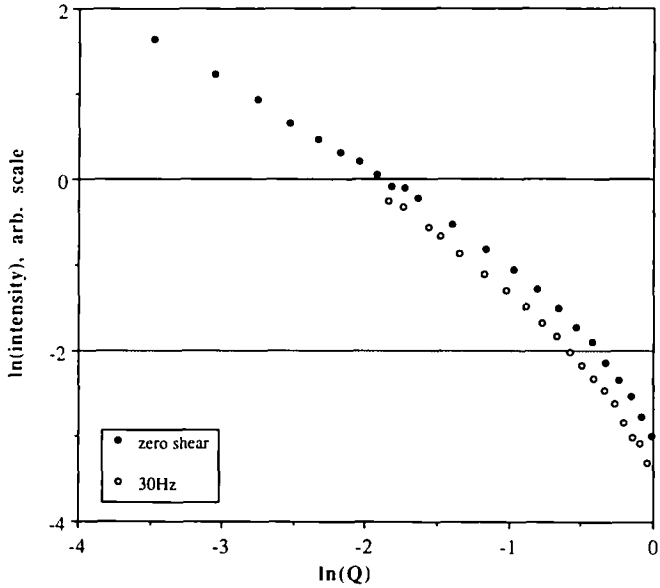

Fig. 4. Circularly averaged intensities evaluated for the micellar solution at equilibrium $\dot{\gamma} = 0.0$ (filled circles) and under shear at $\dot{\gamma} = 30\,s^{-1}$ (open circles). The curves follow a power law slope of -1 over a wide range of Q. The shear data are offset for clarity. The small perturbation in the equilibrium data plot at $\ln Q \sim -2$ results from a slight mismatch between results from two SANS spectrometer detector settings and is insignificant.

micelle behaved as a Gaussian coil [10]; the form factor for a Gaussian coil is

$$(F(Q))^2 = \frac{2}{y^2}[\exp(-y) - 1 + y] \tag{6}$$

where $y = Q^2 R_G^2$ with R_G the radius of gyration given by $R_G^2 = \langle r^2 \rangle / 6$; $\langle r^2 \rangle$ is the mean squared end-to-end chain length. (That the micelles would behave as Gaussian coils seemed possible given the analogy between the worm-like micelle and a real polymer. One could argue further that the worm-like cells might be coiled in some way when the system is at rest, but then uncoil, straighten, and even grow under shear.) Theoretical form factors for these two configurations were evaluated and plotted in Fig. 5, with the plot for a rod included for comparison. The curves are presented as a function of $Q\sigma$, where $\sigma = R$ for the sphere and R_G for the coil, and L for the rod. Here, however, we set $R = L = R_G = 1$. The curves are sufficiently different to conclude that the zero shear data in Fig. 4 are indeed consistent

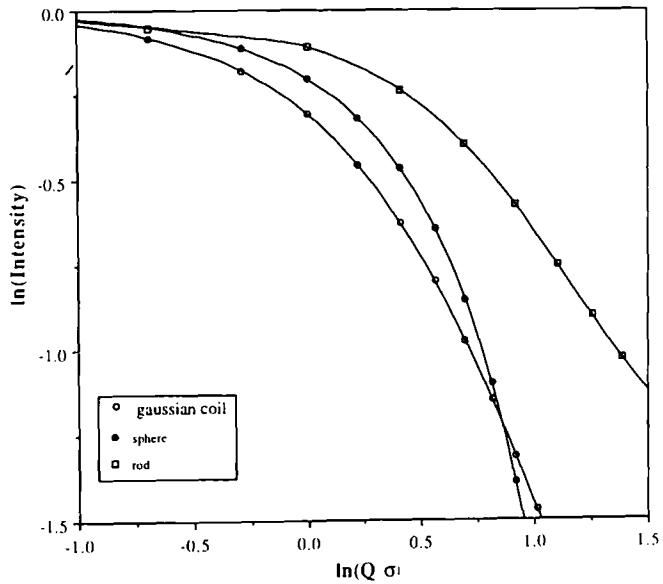

Fig. 5. Theoretical form factor for a sphere, a rod, and a Gaussian coil in equilibrium plotted against $Q\sigma$, where $\sigma = R$ for the sphere, L for the rod, and R_G for the coil.

Table I. Micelle Half-Length Obtained from a Fit of the Scattered Intensity at Various Shear Rates, Using Eqs. (1)–(5) with the Radius Fixed at 2.5 nm

Shear rate (s^{-1})	30	40	50	65	80
L(nm)	375	391	423	389	369

with the pattern expected from rods. From Eq. (2), therefore, we determined a length $2L \approx 200$ nm and a diameter $2a = 50$ nm for the system at rest. The diameter is consistent with previous estimates of the diameter of similar cationic micelles [11].

4.2. Least-Squared Fit of the Shear Data

Intensity data from the shear runs at $\dot{\gamma} = 30$, 40, 50, 65, and 80 s^{-1} were sector averaged and the segments at 90°, 55°, and 0° analyzed given Eqs. (1)–(5) with the length $2L$ and the diameter, $2a$, treated as parameters. Since, however, the radius was found to lie between 2.5 and 2.7 nm at all shears, we set $a = 2.5$ nm (also, consistent with the value found for the system at rest) and refit the data to give L (Table I). The fits were only marginally satisfactory overall. A simultaneous fit of all segments at a given shear gave excellent agreement with data at 90°, but relatively poor agreement at 0° for low Q values.

5. POLYDISPERSITY, CONCLUDING REMARKS

We conclude the paper by speculating why (1) the sheared system at 0° in the x–z plane is poorly fitted and (2) a threshold shear apparently exists. First, we think that polydispersity contributes. It appears that the micelle at rest is rodlike, but its mean length grows to several hundred nanometers on shearing. We hypothesize, however, that the rods are polydisperse in length. A simple model calculation [11] checks this reasoning: namely, the theoretical intensities for a Gaussian distribution of lengths about $L = 1$, given $a = 0.0001$, were calculated for several variances, $\sigma(v)$ at a given shear. Typical results are shown in Fig. 6. Displayed are the $\psi = 0$ (i.e., the x axis in the x–z plane) curves for $\sigma(v) = 0.0$, 0.1, and 0.2 for Γ of Eq. (5) arbitrarily set at 133.3. It is seen that polydispersity flattens the minimum at $QL \sim 3$ and hence thickens the waist of the anisotropic intensity images under shear. The waist is observed experimentally in Figs. 2 and 3 and manifested by the poor fit at $\psi = 0°$, although the fit at $\psi = 90°$ is satisfactory.

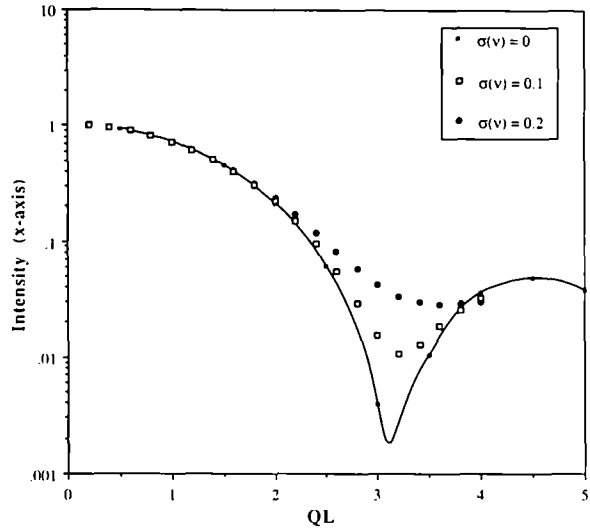

Fig. 6. Intensity for the $\psi = 0$ segment of a scattered intensity plot at $\Gamma = 133.3$ [Eq. (5)] plotted against QL for three values of the polydisperse variance $\sigma(r)$ about $L = 1$: $\sigma(r) = 0.0$, 0.1, and 0.2. The effect of the polydispersity is to thicken the waist of the anisotropic intensity images under shear.

Second, polydispersity could be a cause of a threshold shear. We note that polydispersity has very little effect on the circularly averaged curves at zero shear, so we cannot tell if the growth is uniform from an initial polydisperse configuration or not uniform from a monodisperse base. The former scenario is more plausible. If so, the scattering from polydisperse short rods at low shear will mask anisotropy. Only when an apparent threshold shear is exceeded will the shear rate be high enough, and the rods long enough, to observe anisotropy in the scattering x–z plane. Further work, however, is needed to clarify why the threshold shear exists. Experiments are proposed to study the effect of concentration on a threshold, and to improve the resolution of the scattered data.

ACKNOWLEDGMENT

The NIST contribution to this work was supported in part by Air Force Office of Scientific Research Grant AFOSR-MIPR-94-0027.

REFERENCES

1. R. M. Bain and A. J. Hyde, *Faraday Symp. Chem. Soc.* **5**:145 (1971).
2. H. Rehage and H. Hoffmann, *Faraday Disc. Chem. Soc.* **76**:363 (1983).

3. I. Wunderlich, H. Hoffmann, and H. Rehage, *Rheol. Acta* **26**:532 (1987).
4. J. B. Hayter and J. Penfold, *J. Phys. Chem.* **88**:4589 (1984).
5. J. Kalus, S.-H. Chen, H. Hoffmann, G. Neubauer, P. Lindner, and H. Thurn, *J. Appl. Cryst.* **21**:777 (1988), and references therein.
6. H. J. M. Hanley, G. C. Straty, and F. Tsvetkov, *Langmuir* **10**:3362 (1994).
7. G. C. Straty, *NIST J. Res.* **94**:259 (1989); G. C. Straty, H. J. M. Hanley, and C. J. Glinka, *J. Stat. Phys.* **62**:1015 (1991).
8. S.-H. Chen, *Ann. Rev. Phys. Chem.* **37**:351 (1986).
9. H. C. Van de Hulst, *Light Scattering by Small Particles* (Wiley, New York, 1957); A. Guinier and G. Fourmet, *Small-Angle Scattering of X-Rays* (Wiley, New York, 1955).
10. B. J. Berne and R. Pecora, *Dynamic Light Scattering* (Wiley, New York, 1976).
11. J. Penfold, *J. Appl. Cryst.* **21**::770 (1988).
12. P. S. Goyal, R. Chakravarthy, B. A. Dasannacharya, J. A. E. Desa, and V. K. Kelkar, *Physica B* **156**:471 (1989).